ELSEVIER

Journal of Organometallic Chemistry 661 (2002) 199–209

Journal of Organometallic Chemistry

www.elsevier.com/locate/jorganchem

Time-resolved organometallic photochemistry Femtosecond fragmentation and adaptive control of $CpFe(CO)_2X$ (X = Cl, Br, I)

M. Bergt, T. Brixner, C. Dietl, B. Kiefer, G. Gerber *

Physikalisches Institut, Universität Würzburg, Am Hubland, 97074 Würzburg, Germany

Received 24 June 2002; accepted 23 July 2002

Dedicated to Professor Helmut Werner on the occasion of his retirement in recognition of his tremendous contributions to organometallic chemistry

Abstract

We report a systematic experimental study of the influence of metal–ligand bonding properties on the ultrafast photofragmentation dynamics and on quantum control of organometallic molecules in the gas phase. In the first part, the femtosecond pump–probe technique is combined with reflectron time-of-flight mass spectrometry to record transient mass spectra of the photodissociation products of $CpFe(CO)_2X$ ($Cp = C_5H_5$; X = Cl, Br, I). Sequential dissociation steps are observed for the X = Cl species while concerted and more complex mechanisms are seen in the molecules involving the larger halogens. The overall dissociation rate increases from the lighter toward the heavier halogen ligands in this series which can be explained qualitatively by the different metal–halogen bonding properties and their stabilizing effects on unsaturated intermediate species. In the second part, adaptive quantum control experiments are performed on the X = Cl and X = Br molecules. A femtosecond laser pulse shaper provides spectrally phase-modulated electric fields which are then iteratively optimized by a learning evolutionary algorithm. Direct experimental feedback from the photoproduct mass spectra is used in this search for specific optimization goals. A comparison between the two molecular species shows that laser fields optimized for one molecule also lead to an improvement in the species with the substituted halogen ligand, but not to the same degree as when the substituted molecule is directly optimized. Despite their chemical similarities, adaptive pulse shaping is sensitive enough to detect differences in the investigated metal complexes which are due to the electronic metal–halogen bonding properties. These results suggest an application in chemical analysis where specific signatures are desired for the individual compounds in mixtures of chemically similar molecules.

Keywords: Photodissociation; Femtochemistry; Coherent control; Pulse shaping

1. Introduction

The photochemistry of organometallic compounds has received great attention in the last decades [1,2]. One of the main reasons for such interest is their successful application as photocatalysts in many organic reactions [3–5]. The primary step in these reactions is the generation of unsaturated species by (photo)dissociation of one or several ligands from the saturated organometallic precursor. The efficiency of the primary photolytic step and the chemical nature of the intermediate species are important for the catalytic activity. It would therefore be very helpful to understand the dissociation mechanisms in these molecules on an ultrafast timescale. A number of femtosecond pump–probe experiments on organometallic molecules in the liquid phase have been reported [6–13]. However, little work on the ultrafast dissociation of isolated metalcarbonyl molecules had been done during that time. The first gas-phase experiment with organometallic compounds and femtosecond time resolution was conducted on $Co(CO)_3NO$ in an investigation of vibrational dynamics [14]. Primary photodissociation steps in the gas phase were first examined in $Mn_2(CO)_{10}$ by Zewail and coworkers [15]

* Corresponding author. Tel.: +49-931-8885715; fax: +49-931-8884906

E-mail address: gerber@physik.uni-wuerzburg.de (G. Gerber).

0022-328X/02/$ - see front matter
PII: S0022-328X(02)01821-1

and then in $Fe(CO)_5$ by our group [16,17]. Dissociation dynamics in $Fe(CO)_5$ and the related $Cr(CO)_6$ using different excitation wavelengths were also reported [18,19].

Despite these results, it is generally not clear how the properties of different ligands influence the dissociation dynamics of the parent molecule. However, this knowledge about fragmentation timescales and lifetimes of intermediates, especially the dependence on different types of ligands could presumably be used to 'tune' photochemical properties and hence also catalytic activity. Here we report a first systematic study of ligand influence on organometallic ultrafast photodissociation dynamics [20]. We perform pump–probe studies on the $CpFe(CO)_2X$ ($Cp = C_5H_5$) molecular series under variation of the halogen ligands X = Cl, Br, I.

Another aspect of 'designing' catalytic activity comes into play when considering that bond cleavage is conventionally achieved by intense UV irradiation. However, it would be fascinating if certain metal–ligand bonds could be broken selectively and efficiently, while others were kept intact. This is a possible application of the recently developed technique of adaptive quantum control using specifically shaped femtosecond laser pulses. In this discipline termed 'quantum control' or 'coherent control,' coherent light sources are used to manipulate light–matter interaction by utilizing frequency- and time-domain quantum-mechanical interference phenomena [21–26]. However, since molecular Hamiltonians are usually not known accurately enough, it is not possible to calculate which light field should be optimal for a particular control problem.

A general method to circumvent these problems and to find optimal laser fields under laboratory conditions was proposed by Judson and Rabitz [27]. They suggested a closed-loop scheme involving experimental feedback and an optimization algorithm. This type of experiment was first performed in an experiment by Bardeen et al. [28] where the excited-state population of a laser dye in solution was optimized, and in experiments performed in our group where photodissociation reactions of complex molecules were controlled [29,30]. Other early examples include the excitation of different vibrational modes in a molecular liquid [31] and the control of vibrational dynamics in a four-wave mixing experiment [32]. In the meantime, a number of experiments on adaptive gas-phase control [33–38] have been published, in some works also in connection with pump–probe data [33,36,37]. Selective quantum control was even achieved under liquid-phase conditions [39] and in biological systems [40]. It should be mentioned that optimal quantum control is not limited to molecular systems. Among other applications, femtosecond laser pulse shapers and learning loops have been used for automated pulse compression [41–45] and optimized generation of arbitrary laser pulse shapes [46,47], control of two-photon transitions in atoms [48,49], shaping of Rydberg wavepackets [50], optimization of high-harmonic generation [51], and control of ultrafast semiconductor nonlinearities [52].

Most adaptive quantum control experiments in molecules to date have treated specific optimization goals within one given system. However, it would be very interesting to investigate if the optimized laser fields are really specific to a certain molecule. For this purpose, one should perform systematic studies in series of chemically similar molecules. In the experiments reported here, we use adaptive femtosecond quantum control to investigate the differences and similarities in the molecular species $CpFe(CO)_2X$ (X = Cl, Br). This will demonstrate the sensitivity of adaptive pulse shaping on the detailed electronic properties of the investigated molecule.

2. Experimental

2.1. General scheme

The experimental setups of the pump–probe and the automated control experiment are shown schematically in Fig. 1 and will be discussed separately below. The light source employed in both experiments is a Ti–Sapphire chirped-pulse amplification (CPA) laser system providing 80-fs, 1-mJ laser pulses at a center wavelength of 800 nm and at a repetition rate of 1 kHz. The laser pulses (emerging either from the pump–probe or the pulse-shaper setup) are focused into an effusive beam of the target molecules $CpFe(CO)_2X$ (X = Cl, Br, I) using a 300-mm quartz lens. Ionic mass spectra of the fragment patterns following multiphoton laser excitation are collected using a reflectron time-of-flight mass spectrometer (RETOF). The molecular beam is generated by evaporating a sample of either of the molecules $CpFe(CO)_2X$ (X = Cl, Br, I) separately in the case of the pump–probe experiments, or by preparing a mixture of $CpFe(CO)_2X$ (X = Cl, Br) in the case of the automated control experiments. For this purpose, the samples are heated in a glass tube to a temperature of ca. 80 °C, and the vapor is expanded through a 0.5-mm glass nozzle.

The structural formula for the investigated molecules is indicated in Fig. 1 (inset). Three different types of metal–ligand bonds are found in this molecule: two Fe–CO bonds, the η^5-Fe–Cp bond and the Fe–X bond. In this saturated complex, the eight d-electrons of the iron atom form a stable 18-electron configuration together with the valence electrons of the ligands. Photochemical investigations on these molecules under liquid-phase conditions and in matrices showed that after UV excitation either the halogen ligand X is split off or

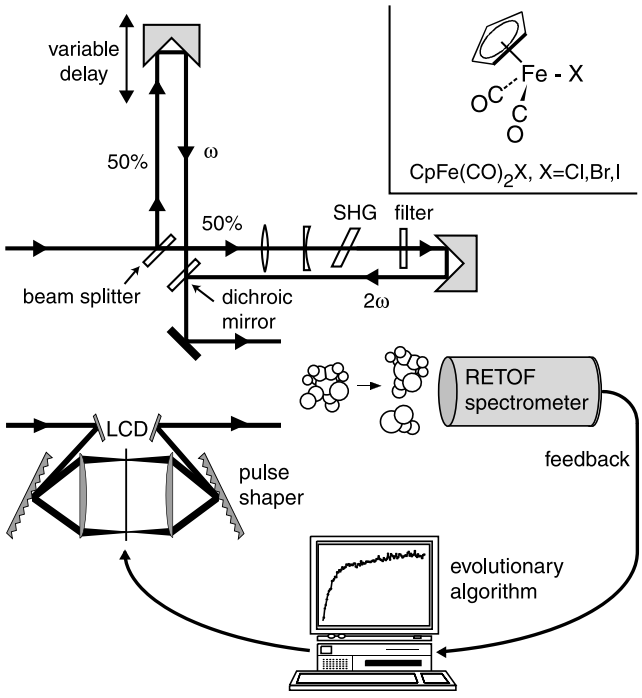

Fig. 1. Experimental set up. Top part: time-resolved mass spectrometry is conducted by providing 400 nm pump and 800 nm probe laser pulses with a Mach–Zehuder interferometer. The probe arm can be delayed using a computer-controlled delay stage. After recombination, the pump and probe laser pulses are focussed into the interaction region of a RETOF spectrometer. Bottom part: for the automated quantum control experiment, a computer-controlled pulse shaper generates arbitrarily tailored femtosecond laser pulses. The experimental outcome (the photodissociation product yield) obtained with these pulses is used as feedback in an evolutionary algorithm. The electric field of the laser pulses is iteratively optimized until an optimal result is found. Inset: The chemical structure of the molecules $CpFe(CO)_2X$ is indicated. The Cp ring (C_5H_5) is η^5-connected to the central iron atom.

the Fe–CO bond is broken [53–59]. Furthermore, isomerization reactions and intraligand rearrangements are possible. However, time-resolved experiments clarifying the primary reactive steps after photoexcitation have not been reported so far. These primary events are the focus of the experiments reported here.

2.2. Femtosecond time-resolved mass spectrometry

In the time-resolved experiment, the 800-nm laser beam is split into two identical parts (Fig. 1, top part) within a Mach–Zehnder interferometer. In one arm of the interferometer the 400-nm pump laser pulses are produced by second-harmonic generation (SHG) in a 100-μm BBO crystal. The 800-nm probe pulses in the other arm can be delayed with respect to the pump pulses using a computer-controlled translation stage. Pump and probe laser pulses are combined collinearly with a dichroic mirror. Transient ionization spectra are collected for all fragments simultaneously by measuring complete mass spectra at different time delays with a transient recorder.

The time delay is varied in steps of 5 fs between −500 and +1000 fs. At each point, mass spectra are averaged over 100 laser shots to reduce shot-to-shot fluctuations. The effects of longer-term variations are reduced by recording the complete transients several times and averaging again. This leads to a significant improvement in the signal-to-noise ratio. The energies of both the pump and the probe laser pulses are attenuated such that the ionic signals generated by either laser pulse alone are insignificantly small as compared to the combined pump–probe signal.

The recorded transients of the individual mass peaks are then evaluated with a rate model to extract timescales of formation of intermediate states involved in the fragmentation of $CpFe(CO)_2X$. In the scenario of our experiments, the 400-nm pump laser pulse prepares population on an electronically excited neutral intermediate state of the parent molecule $CpFe(CO)_2X$. The dissociation process could then in principle be described by the ensuing wavepacket propagation if the multidimensional potential energy surfaces (PES) for the complete reaction pathway were available. Experimental evidence could then be used to test the predictions of different PES models. However, for the investigated molecules the PES are not yet known although some work is in progress [60]. In order to obtain at least some information on the kinetics of the photodissociation process, the neutral dissociation is described by a simple rate model. Although this is not the correct dynamical description employing PES, the recorded transients are nevertheless reproduced well with this model (at the available experimental time resolution).

In our case, after initial excitation the population in the parent molecule decreases because of first dissociative steps, e.g. $CpFe(CO)_2X^* \rightarrow CpFeCOX^*$. We assume the population of an intermediate state to decay exponentially with a rate k or a corresponding time constant $\tau = 1/k$, while the product state is populated with the same rate. Similarly, the product CpFeCOX* is able to undergo further fragmentation. Within the probe step, the distribution of neutral fragments at delay time t is transferred to the ionic continuum by 800-nm multiphoton ionization and detected in the mass spectrometer. The timescale of formation of a certain neutral intermediate species is in principle determined by the shape of the transient ion signal for the same mass. In summary, we can describe the photodissociation process for example as:

$$CpFe(CO)_2X \xrightarrow{\tau_1} CpFeCOX^* \xrightarrow{\tau_2} CpFeX^* \xrightarrow{\tau_3} \ldots$$

However, two other contributions to possible fragment ion production have to be considered: (i) ions can be formed by the pump or probe laser alone; and (ii)

ions generated during the above scenario can undergo further fragmentation, thus appearing in the transients of different intermediate species. The first case results in a constant offset in the ionic transients which can be avoided by careful energy attenuation as already mentioned above. The ionic species generated in the second case carry the dynamics of the intermediate species they were originally drawn from by 800-nm multiphoton ionization. In other words, the transient signal of a certain ionic fragment is a combination of all preceding dissociation steps.

In order to address this, data modeling starts with the transient of the parent ion $CpFe(CO)_2X^+$. The rate found during this first step is assigned to the dissociation of the neutral excited parent molecule $CpFe(CO)_2X^*$. In a second step we try to discover this rate in the transient of the ionic fragment with smaller mass, e.g. $CpFeCOX^+$. If this fragment transient can already be modeled using the rate from the parent molecule, the transient is assumed to consist only of contributions from fragmentation of preceding ions. However, if an additional rate is needed, a new intermediate state is assigned, in the example given here $CpFeCOX^*$. By successive application to all ionization transients, the complete information about the dissociation process can be extracted.

Fitting of the data is done with a nonlinear Levenberg–Marquardt procedure [61]. The time resolution of the experiment is taken into account by convoluting the exponential molecular response functions with a Gaussian apparatus response function due to the finite duration of the pump and probe laser pulses. Since the order of the multiphoton processes relevant to the photodissociation reactions is not exactly known, a measured cross-correlation is only an approximation for the apparatus response function. Therefore, this time constant is also determined in the fitting procedures directly from the ionic transients.

2.3. Adaptive quantum control

The automated control experiment is performed using computer-controlled frequency-domain pulse shaping [62–67] in combination with an evolutionary algorithm (Fig. 1, bottom part). The setup of our pulse shaper has been described previously [42,44]. It consists of a zero-dispersion compressor in 4f geometry, which is used to spatially disperse and recollimate the femtosecond laser spectrum. Arbitrary pulse shapes can be generated by applying different voltages to the 128 pixels of a liquid-crystal display (LCD) placed in the Fourier plane of the compressor. Upon transmission of the laser beam through the LCD a frequency-dependent phase is acquired due to the individual pixel voltage values. In this configuration the spectral amplitudes remain unchanged and thus the pulse energy remains constant for the different pulse shapes. In order to find the optimal electric fields required to trigger a specific reaction in the target molecules, a global search algorithm is used. Following a suggestion by Judson and Rabitz [27] we implement an iterative learning loop to search for optimized electric fields. At each iteration the experimental outcome for a specific pulse shape, i.e. the amount of a certain ionic mass fragment, is evaluated with respect to the optimization goal. The global search method used for this purpose is an evolutionary algorithm [68,69]. Our implementation was described in detail elsewhere [42].

In this experiment, boxcar integrators are used to record the product yields of those ionic fragments entering in the optimization function. For each laser pulse shape, the signal is averaged over 1000 laser shots. At the end of the optimization, complete mass spectra are recorded and analyzed by applying again the best pulse shape of the final generation. The pulse energy in the optimization experiments is set to ca. 130 μJ.

3. Investigation of fragmentation dynamics

3.1. Results

Mass spectra of the three investigated molecules $CpFe(CO)_2X$ (X = Cl, Br, I) are shown in Fig. 2. They have been recorded using 800-nm laser pulses of duration 80 fs and a peak intensity of ca. 10^{13} W cm^{-2}. The characteristic features within each mass peak cluster are due to natural isotope distributions. In the $CpFe(CO)_2Cl$ series (Fig. 2a) the isotope peaks arising from ^{35}Cl and ^{37}Cl abound at an expected ratio of 3:1, whereas in the $CpFe(CO)_2Br$ molecule (Fig. 2b) the two isotopes ^{79}Br and ^{81}Br are distributed with ca. equal heights. The iodine atom has only one natural isotope, and therefore the isotopic structure in $CpFe(CO)_2I$ (Fig. 2c) is given by the isotopes of Fe and C alone. The mass spectrum of $CpFe(CO)_2Br$ also shows contributions of Cl-containing species because of small impurities remaining in the molecular beam machine from previous measurements on $CpFe(CO)_2Cl$.

In all three mass spectra the molecular parent ion $CpFe(CO)_2X^+$ is visible. Furthermore, a number of ionic fragments are produced in two distinct fragmentation channels. In the first channel, the halogen ligand X remains bounded to the complex, leading to the fragment ions $CpFe(CO)_{1,0}X^+$ whereas the second channel is characterized by those fragments in which the halogen ligand X is lost as a primary step, leading to the fragment ions $CpFe(CO)^+_{2,1,0}$. Additional photoproducts are given by the Cp ring and its fragments as well as their combinations with Fe. Comparing the mass spectra of the three molecules $CpFe(CO)_2X$ qualitatively, a systematic variation in the relative fragment abundances

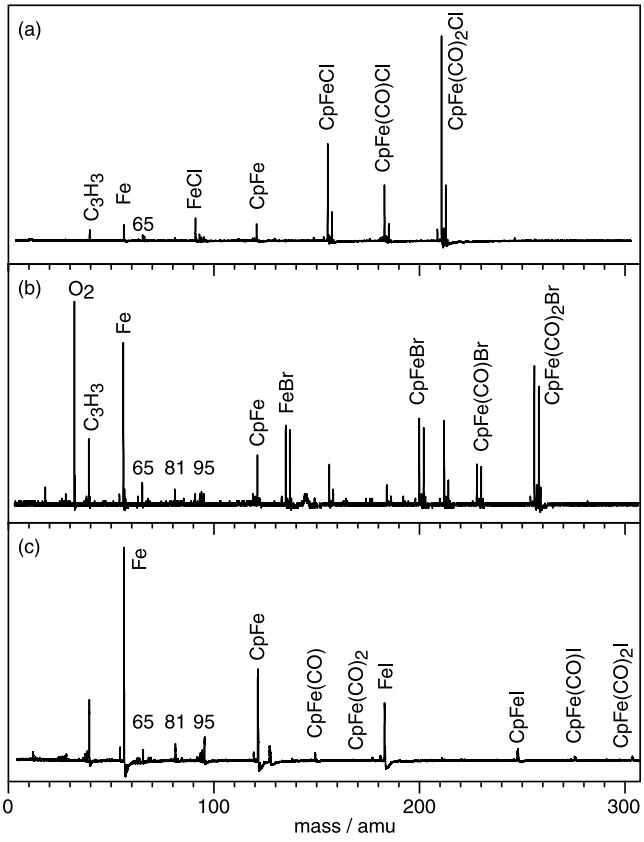

Fig. 2. Mass spectra of $CpFe(CO)_2X$ for: (a) X = Cl; (b) X = Br; (c) X = I, recorded with 800 nm laser pulses of duration 80 fs and a peak intensity of ca. 10^{13} W cm^{-2}.

can be observed. In the $CpFe(CO)_2Cl$ series, the mass peak heights decrease from the heavier toward the lighter fragments, whereas in the $CpFe(CO)_2Br$ series, all fragment peaks have ca. the same height. Finally in the $CpFe(CO)_2I$ species, predominantly smaller fragments are observed under the given experimental conditions.

The investigation of photodissociation dynamics was carried out performing 400-nm-pump–800-nm-probe experiments on each of the $CpFe(CO)_2X$ molecular species separately. The evaluation was then carried out by employing the rate model described in Section 2.2. Since the cross-correlation width is on the order of 100 fs, it cannot be decided if coherent wavepacket oscillations on a shorter timescale are superimposed on the observed transients. Better time resolution would be required to answer that and to ultimately investigate the nature of the fragmentation process, i.e. to decide if the rate model is sufficient or if 'ballistic' wavepacket motion needs to be considered. Nonetheless, some general conclusions can be drawn from the following experiments as it is still possible to extract dissociation times from the recorded transients, and the experimental data reported here are nicely reproduced by the rate model.

Transients of the $CpFe(CO)_2Cl$ photoproducts are shown in Fig. 3. Since the decay starts with the parent molecule, its transient can be fitted by a monoexponential decay at a time constant of (40 ± 10) fs convoluted with the response function of the apparatus at an FWHM of (100 ± 10) fs.

The $CpFeCOCl^+$ transient differs from that of the parent molecule in the decaying shoulder. Two contributions have to be considered here. On the one hand, ionic fragmentation can lead from $CpFe(CO)_2Cl^+$ to $CpFeCOCl^+$ (dashed curve). But this is not sufficient to explain the observed $CpFeCOCl^+$ transient and an additional neutral CpFeCOCl intermediate has to be assumed (dashed–dotted curve). The fit yields a rise time of (40 ± 10) fs and a decay time of (90 ± 15) fs. The rise time corresponds to the decay time of the neutral excited-state intermediate of the parent molecule, i.e. the rate of CpFeCOCl build-up. The decay time for $CpFeCOCl^+$ suggests further fragmentation under additional CO ligand loss.

The $CpFeCl^+$ transient contains two ionic contributions from the $CpFe(CO)_{2,1}Cl^+$ transients (dashed lines) as well as an additional neutral contribution showing a

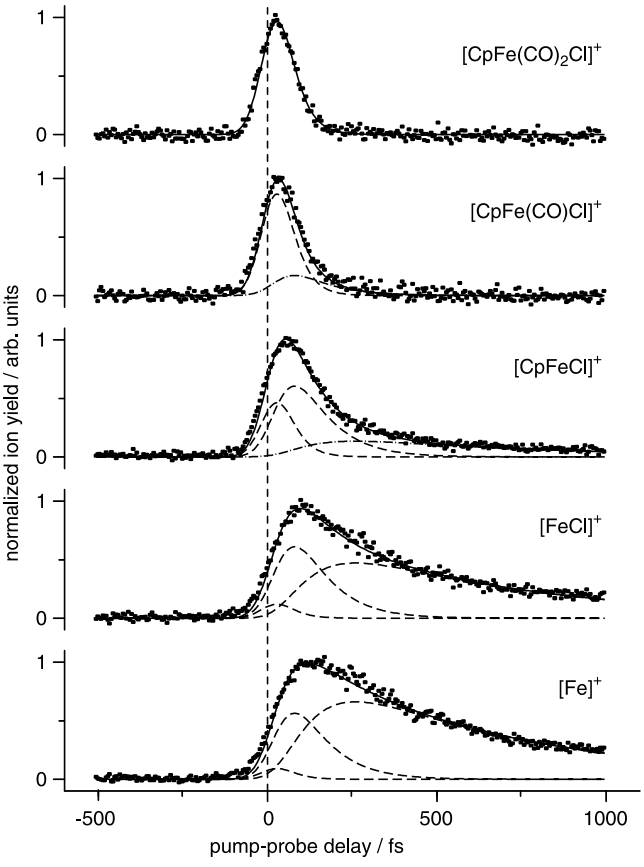

Fig. 3. $CpFe(CO)_2Cl$ transients. The experimental data points (solid squares) are fitted by the molecular response function from the rate model (solid lines). The individual contributions from neutral fragmentation (dashed–dotted lines) and ionic fragmentation (dashed lines) are also shown.

decay time of (800 ± 50) fs (dashed–dotted line). Therefore, an additional neutral intermediate corresponding to CpFeCl has to be assumed. The conclusion from these observations is that upon excitation with 400-nm laser pulses, $CpFe(CO)_2Cl$ shows sequential fragmentation of the two CO ligands within ca. 40 fs + 90 fs = 130 fs via the neutral CpFeCOCl intermediate.

The $FeCl^+$ and the Fe^+ transients can be explained purely by ionic contributions from the $CpFe(CO)_{2,1,0}Cl^+$ transients and do not require additional neutral intermediates. This means that the product of the CpFeCl decay—which should be produced with a characteristic time of (800 ± 50) fs—cannot be identified. The most likely candidate would be FeCl. However, the $FeCl^+$ transient shows only ionic contributions.

The second fragmentation channel mentioned above, where the primary dissociation step corresponds to the loss of the halogen ligand, is not a dominant pathway in the $CpFe(CO)_2Cl$ species (nor in the $CpFe(CO)_2Br$ species), and the statistics in the observed transients were not good enough to extract time constants.

Transients for the $CpFe(CO)_2Br$ molecule and its photoproducts are shown in Fig. 4. The apparatus response function has an FWHM of (140 ± 10) fs, which broadens the transients as compared to those of the $CpFe(CO)_2Cl$ species. The difference arises because these experiments were conducted on a different day with slightly different laser characteristics. The overall results of the data evaluation are similar to those of the $CpFe(CO)_2Cl$ molecule. However, the $CpFeBr^+$ transient does not require a neutral contribution in the fitting procedure. The neutral intermediate is found in the $FeBr^+$ transient instead. Therefore, the parent molecule $CpFe(CO)_2Br$ decays within (45 ± 10) fs under CO ligand loss into CpFeCOBr which in turn decays with a time constant of (100 ± 30) fs. The subsequent decay of FeBr occurs within (450 ± 40) fs.

Finally, the $CpFe(CO)_2I$ transients are shown in Fig. 5. The apparatus response function has a width of (150 ± 10) fs. In this molecule, the $CpFe(CO)_2I^+$ and the $CpFeCOI^+$ transient are identical. In both curves, a decay time constant of (45 ± 10) fs is extractable. This means that no neutral CpFeCOI intermediate could be found. But for both the $CpFeI^+$ and the FeI^+

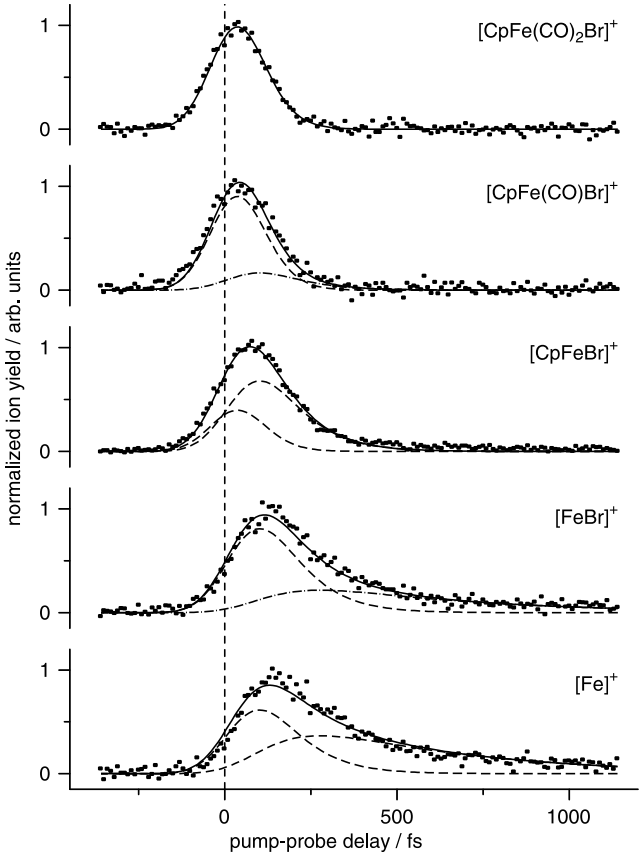

Fig. 4. $CpFe(CO)_2Br$ transients. The experimental data points (solid squares) are fitted by the molecular response function from the rate model (solid lines). The individual contributions from neutral fragmentation (dashed–dotted lines) and ionic fragmentation (dashed lines) are also shown.

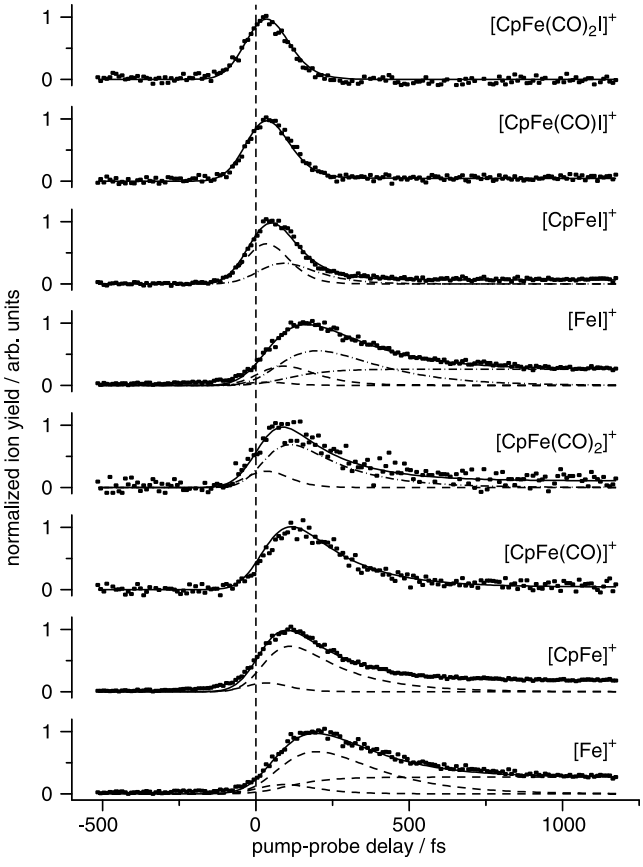

Fig. 5. $CpFe(CO)_2I$ transients. The experimental data points (solid squares) are fitted by the molecular response function from the rate model (solid lines). The individual contributions from neutral fragmentation (dashed–dotted lines) and ionic fragmentation (dashed lines) are also shown.

transients, neutral contributions have to be assumed, corresponding to lifetimes in the neutral intermediates of (85±10) and (190±15) fs, respectively. Some fraction of the neutral FeI molecules do not decay further, which leads to a plateau region in the corresponding FeI^+ transient.

In addition to this first fragmentation channel, the primary halogen ligand-loss channel plays an important role in the $CpFe(CO)_2I$ molecule. Apart from the ionic contributions from the parent, the $CpFe(CO)_2^+$ transient shows a biexponential behaviour with a rise time of (45±10) fs and a decay time of (180±20) fs. The rise time corresponds to the decay time of the neutral intermediate in the parent molecule. The $CpFeCO^+$ and the $CpFe^+$ transients are explained by purely ionic contributions. This suggests that the corresponding neutral fragments CpFeCO and CpFe decay faster than being produced by fragmentation of $CpFe(CO)_2$.

3.2. Discussion and dissociation model

In the photodissociation of $CpFe(CO)_2X$ (X = Cl, Br, I) after excitation with 400-nm femtosecond laser pulses, two fragmentation channels for the parent molecule have to be discriminated: $CpFe(CO)_2X \rightarrow CpFeCOX + CO \rightarrow \ldots$ and $CpFe(CO)_2X \rightarrow CpFe(CO)_2 + X \rightarrow \ldots$. In all three molecular species, the parent molecule decays within 40–50 fs into these two channels. Predominantly, the primary process of CO ligand loss is observed, and the halogen ligand remains bounded throughout the dissociation process (first channel). Only in the $CpFe(CO)_2I$ species, the halogen-free series of photoproducts $CpFe(CO)_{2,1,0}$ (second channel) is significant.

In the halogen-containing fragmentation series, a sequence of CO and Cp losses is found. The timescales for these steps are different in the three investigated molecular species. A comparison is given in Fig. 6. In the $CpFe(CO)_2Cl$ molecule, ultrafast but sequential losses of the first and the second CO ligands within 40 and 90 fs, respectively, are observed. On a longer timescale of 800 fs, the Cp ring is split off. The complete dissociation of the $CpFe(CO)_2Cl$ molecule up to FeCl therefore takes ca. 930 fs.

In the $CpFe(CO)_2Br$ molecule the first CO ligand loss occurs within 45 fs. However, in contrast to the $CpFe(CO)_2Cl$ species, the subsequent dissociation of the Cp ring and the loss of the second CO group occur simultaneously within 100 fs. This concerted ligand-loss pathway taking place in CpFeCOBr is the main difference to the sequential process in CpFeCOCl. The total dissociation time for $CpFe(CO)_2Br$ including the last step of FeBr fragmentation (450 fs) is therefore ca. 600 fs.

Finally, in the case of $CpFe(CO)_2I$, sequential cleavage of Fe–CO bonds is not seen. The two CO ligands rather dissociate in a concerted manner, and the subsequent dissociation steps proceed faster than in the cases of either $CpFe(CO)_2Cl$ or $CpFe(CO)_2Br$. Complete fragmentation of $CpFe(CO)_2I$ takes only about 320 fs. However, a significant amount of the FeI population does not decay at all (in the investigated timescale of 1.5 ps) and leads to an asymptotic plateau in the corresponding transient. This plateau is of much less importance in the $CpFe(CO)_2Cl$ and $CpFe(CO)_2Br$ species.

On total, the halogen-containing fragmentation series proceeds slowest for $CpFe(CO)_2Cl$. The rate of complete fragmentation of the molecule increases throughout the series of compounds so that the fastest dissociation is found for $CpFe(CO)_2I$. The halogen-free fragmentation series is most important in the $CpFe(CO)_2I$ species, where $CpFe(CO)_2$ is produced within 45 fs and decays within 180 fs.

The differences in the total dissociation timescales can be explained by considering the electronic properties of the metal–halogen bonds. Our experiments show that the primary process in all three molecules is the loss of at least one CO ligand. This step produces unsaturated 16-valence-electron complexes. The relatively small size of the chlorine orbitals results in a good overlap with the metal orbitals, and hence provides for an efficient mechanism of electron backtransfer from the halogen

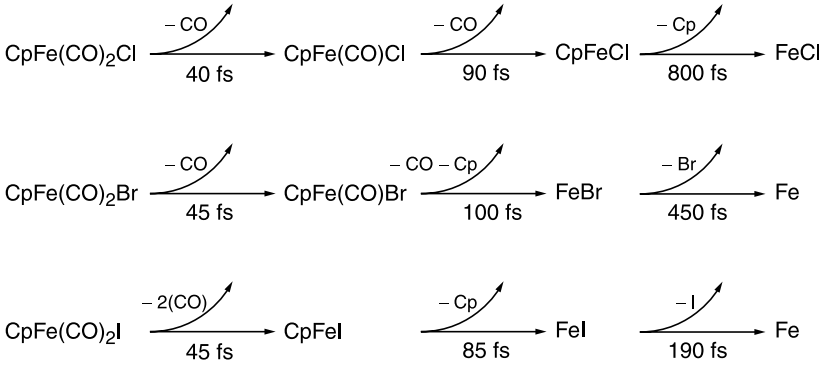

Fig. 6. Dissociation model for $CpFe(CO)_2X$ (X = Cl, Br, I). The decay timescales are given for the three molecular species as extracted from the pump–probe transients of Figs. 3–5. Only the fragmentation channel characterized by initial CO loss is shown.

ligand toward the metal center. This process leads to a stabilization of the intermediate unsaturated species and therefore to a reinforcement of the remaining bonds. As a consequence, the dissociation is slowed down. For the larger iodine orbitals, the overlap with the metal orbitals is not as efficient and the stabilizing effect of the electron backtransfer is much weaker. This explains the observation that in the $CpFe(CO)_2I$ molecule both CO ligands dissociate simultaneously after excitation. An intermediate case is found for $CpFe(CO)_2Br$. Here, the second CO-dissociation step occurs sequential to the first CO loss because of better stabilization of the intermediate as compared to $CpFe(CO)_2I$. However, the Cp ligand in $CpFe(CO)_2Br$ is dissociated simultaneously with the second CO group, indicating that the stabilization is not as good as in $CpFe(CO)_2Cl$.

The primary halogen–metal bonding (before any dissociation has occurred) is strongest for $CpFe(CO)_2Cl$ and weakest for $CpFe(CO)_2I$ as can be seen by comparing the corresponding binding energies [70]. This explains the fact why the fragmentation series with primary halogen loss is more pronounced in the iodine case than in the chlorine and bromine species. Furthermore, in the halogen-containing fragmentation series the final dissociative step of halogen–ligand abstraction occurs faster for FeI (190 fs) than for FeBr (450 fs) as expected. In the case of FeCl, the dissociation is not seen at all in the observed time window, again in accordance with the expectations from the binding energies.

4. Photoproduct control

The experiments discussed in the previous section have shown that the properties of the halogen ligand influence the complete fragmentation dynamics of the investigated series of metal complexes. Despite the chemical similarities between the three molecules, the different electronic properties of the ligands play an important role in the nature of the photoinduced wavepacket dynamics and the resulting dissociation timescales. In the following it will be investigated if these differences are also visible in adaptive quantum control experiments.

In the first experiments on adaptive quantum control of chemical reactions, the molecular species $CpFe(CO)_2Cl$ was investigated and the ratio of the two photoproduct yields of $CpFeCOCl^+$ versus $FeCl^+$ was controlled [30]. Specific laser pulse shapes were found by evolutionary optimization using experimental feedback. These laser pulses were able to either increase or decrease the $CpFeCOCl^+/FeCl^+$ ratio with respect to the value achieved by bandwidth-limited laser pulses. The question of complexity in these types of control problems was analyzed in another experiment where the number of optimization parameters was reduced systematically [34]. It was found that best optimization results were achieved with the maximum number of the available 128 independent parameters, whereas reduction to 64 or 32 parameters resulted in inferior $CpFeCOCl^+/FeCl^+$ ratios. Furthermore, the absence of correlations between the optimization goal and the yield of second-harmonic generation showed that the control mechanism cannot be explained by simple intensity variation of the applied laser fields [34]. Specific electric field structures are required instead.

As another way to investigate the specificity of the optimized laser pulse shapes, we here investigate their performance on chemically similar molecules. For this purpose, a mixture of $CpFe(CO)_2Cl$ and $CpFe(CO)_2Br$ was prepared simultaneously in one molecular beam. In the first part of the experiment, the optimization goal was set as maximization of the $CpFeCOCl^+/FeCl^+$ ratio just as in the control experiments published previously [30]. The evolution of the feedback signal (i.e. in the language of evolutionary algorithms the so-called 'fitness' of the best individual of one population) is shown in Fig. 7a as a function of generation number within the evolutionary algorithm, employing 128 independent optimization parameters. A clear increase in the product ratio is seen. We then performed a maximization of the $CpFeCOBr^+/FeBr^+$ ratio under identical experimental conditions where a qualitatively similar evolution of the feedback signal is observed (Fig. 7b). In both cases the optimized branching ratios are higher than the ratios achieved with unshaped laser pulses, indicating successful learning.

The two molecular systems are now compared by investigating how the electric field optimized for the $CpFeCOCl^+/FeCl^+$ branching ratio influences the $CpFeCOBr^+/FeBr^+$ ratio and vice versa. For this purpose the mass spectra produced by the best individuals of the final generations of Fig. 7 are evaluated and the results summarized in Fig. 8. After maximizing the $CpFeCOCl^+/FeCl^+$ ratio, its value (column A) is significantly increased with respect to unshaped laser pulses (dashed black line). Using this same laser pulse shape on the $CpFe(CO)_2Br$ molecule, the value of the corresponding $CpFeCOBr^+/FeBr^+$ ratio is increased as well (column B) with respect to unshaped pulses (dashed white line). This indicates the chemical similarities between the two molecules, i.e. an optimally controlled photoproduct branching ratio in $CpFe(CO)_2Cl$ also leads to an improvement in $CpFe(CO)_2Br$. The overall lower absolute $CpFeCOBr^+/FeBr^+$ ratio as compared to $CpFeCOCl^+/FeCl^+$ was already discussed in the previous section and is not the main focus here.

The sensitivity of the adaptive quantum control approach on detailed electronic structure is now seen when comparing these findings with a direct optimization in the $CpFe(CO)_2Br$ molecule. Whereas the

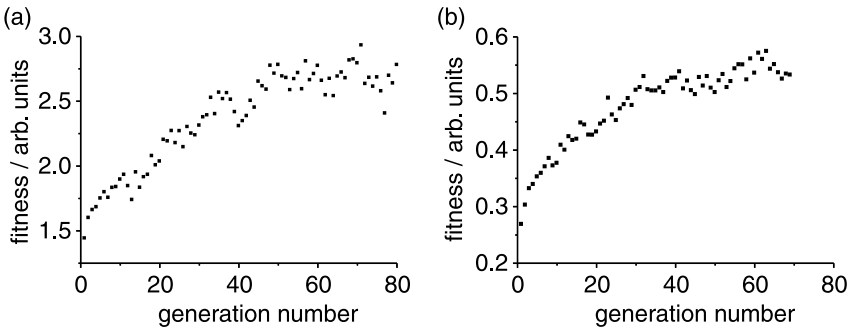

Fig. 7. Evolution of feedback signal (i.e. 'fitness value ' of best individual laser pulse shape within one generation) as a function of generation number. The optimizations performed are: (a) maximization of the $CpFeCOCl^+$–$FeCl^+$ photoproduct yield ratio; and (b) maximization of the $CpFeCOBr^+/FeBr^+$ ratio.

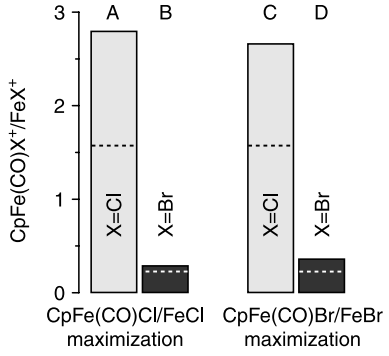

Fig. 8. Comparison of adaptive quantum control experiments on $CpFe(CO)_2X$ (X = Cl, Br). The $CpFeCOX^+/FeX^+$ ratios are shown for both the $CpFeCOCl^+/FeCl^+$ maximization (columns A and B) and the $CpFeCOBr^+/FeBr^+$ maximization (columns C and D) as indicated (for halogen ligand X = Cl: columns A and C, for X = Br: columns B and D). The branching ratios achieved with unshaped femtosecond laser pulses are indicated by dashed lines.

$CpFeCOBr^+/FeBr^+$ ratio had already been increased in the $CpFeCOCl^+/FeCl^+$ optimization (column B), direct maximization of $CpFeCOBr^+/FeBr^+$ further improves on this result and leads to a higher ratio (column D). This means that the learning algorithm is able to find laser pulse shapes which are specifically adapted to the ligand substitution Cl → Br. At the same time, the laser pulse optimized for a high $CpFeCOBr^+/FeBr^+$ ratio also increases the $CpFeCOCl^+/FeCl^+$ branching (column C). However, the value after direct $CpFeCOCl^+/FeCl^+$ optimization (column A) is not quite achieved. This situation is equivalent to the situation discussed above in that the laser pulse shape optimized for one molecule also improves the corresponding pathway in the other molecule because of the chemical similarities, but not to the same value because of the remaining molecular differences.

From the quantum control experiments on $CpFe(CO)_2Cl$ and $CpFe(CO)_2Br$ it can be concluded that adaptive femtosecond pulse shaping is able to discover laser fields which are specifically optimized for a given molecule. Of course it would be desirable to interpret these optimal fields on the basis of the pump–probe experiments and e.g. to decide which role is played by the different fragmentation channels in the optimization results. For example, it is in general still an open question in optimal control experiments how important the channels of ionic fragmentation versus neutral fragmentation followed by ionization really are. In the pump–probe experiments and their evaluation using the rate model, the transient signals were explained by a combination of all processes. One can therefore not expect to distinguish the role of these channels in adaptive control experiments by simply analyzing the optimized electric fields. Nonetheless, the results reported here indicate the sensitivity of the adaptive control method on detailed electronic properties even in chemically very similar molecules.

5. Conclusion

The influence of different halogen ligands X (X = Cl, Br, I) on the photodissociation mechanisms of the transition metal complexes $CpFe(CO)_2X$ have been investigated by combination of the femtosecond pump–probe technique with reflectron time-of-flight mass spectrometry in molecular beams. Furthermore, adaptive quantum control with shaped femtosecond laser pulses was employed to investigate which effect ligand substitution has on the control of photoproduct branching ratios.

In the pump–probe experiments it was found that the nature of the halogen ligand has a clear influence on the dissociation kinetics of the whole molecule, even on the fragmentation times of those bonds where the halogen ligand is not directly involved. Our data indicate that the rate of complete fragmentation of the molecule is slowest for the X = Cl species (ca. 930 fs) and increases throughout the series to the X = Br (ca. 600 fs) and the X = I species (ca. 320 fs). Furthermore, while sequential dissociation steps are observed for the X = Cl species,

concerted and more complex mechanisms are seen for molecules containing the larger halogens. A simple qualitative explanation for this behaviour can be given by considering the nature of the unsaturated complex generated in the initial steps of the dissociation process. Electron backtransfer mechanisms may be responsible for stabilization of intermediate compounds. This is more effective for the lighter halogen ligands and hence leads to longer dissociation timescales. These observations suggest that in gas-phase photoreactions, the timescales and mechanisms of fragmentation can be modified and possibly tuned by changing the electronic properties of the metal–halogen bond.

In addition to these experiments on dissociation kinetics, the recently developed technology of adaptive femtosecond pulse shaping was employed to control photoproduct branching ratios in the molecules $CpFe(CO)_2Cl$ and $CpFe(CO)_2Br$. A learning algorithm used direct feedback from the experimentally recorded mass spectra to iteratively improve the phase function of laser pulses such that finally a particular control objective was realized. Specifically, we were interested in the influence of the halogen ligand on the dissociation characteristics of the molecules and on the control of those branching ratios where not even a metal–halogen bond is broken. For this purpose, we investigated the performance of a laser pulse shape optimized for one type of halogen ligand when applied to the molecule with the other halogen atom. It was found that laser pulses optimal for one molecule also increase the corresponding branching ratio in the other species. This behaviour indicates the chemical similarities between the different molecules of the series. However, the branching ratio of the related molecule is not increased as much as when it is directly optimized. This points at the detailed electronic differences between the two species arising from the nature of the halogen ligands. Adaptive femtosecond pulse shaping is obviously sensitive enough to discover and exploit these differences. A quantitative understanding of both the pump–probe transients and the results in the adaptive quantum control experiment requires detailed quantum dynamical calculations.

Finally, the adaptive control results can be related in a very general sense to experiments we have recently conducted in a solution–phase environment [39]. There, we found that chemically very different molecules which show the same linear absorption profiles can nevertheless be specifically excited (i.e. one molecule preferably with respect to the other) using femtosecond pulse shaping. Adaptive control was able to exploit differences in the photoinduced wavepacket dynamics. In the experiments conducted here, adaptive control is able to find pulse shapes which are specific even for chemically very similar molecules. This feature might have an application in chemical analysis where one would like to obtain some kind of 'signature' selectively from one compound in a mixture of different substances.

Acknowledgements

The organometallic substances have been synthesized in the group of W. Malisch who also participated in the interpretation of the results. Furthermore, we thank N.H. Damrauer for many helpful discussions. In addition to scientific cooperation, we had financial support from the SFB 347 at the University of Würzburg: 'Selective Reactions of Metal-Activated Molecules', the European Coherent Control Network (COCOMO): HPRN-CT-1999-00129, and the 'Fonds der Chemischen Industrie'.

References

[1] M.S. Wrighton, Chem. Rev. 74 (1974) 401.
[2] G.L. Geoffroy, M.S. Wrighton, Organometallic Photochemistry, Academic Press, London, 1979.
[3] M.S. Wrighton, D.S. Ginley, M.A. Schroeder, D.L. Morse, Pure Appl. Chem. 41 (1975) 671.
[4] I. Wender, P. Pino (Eds.), Organic Synthesis via Metal Carbonyls, vol. 1+2, Wiley, New York, 1977.
[5] D.C. Bailey, S.H. Langer, Chem. Rev. 81 (1981) 110.
[6] A.G. Joly, K.A. Nelson, J. Phys. Chem. 93 (1989) 2876.
[7] P.A. Anfinrud, C.H. Han, T.Q. Lian, R.M. Hochstrasser, J. Phys. Chem. 95 (1991) 574.
[8] T.P. Dougherty, E.J. Heilweil, Chem. Phys. Lett. 227 (1994) 19.
[9] A. Waldman, S. Ruhman, S. Shaik, G.N. Sastry, Chem. Phys. Lett. 230 (1994) 110.
[10] N.J. Tro, J.C. King, C.B. Harris, Inorg. Chim. Acta 229 (1995) 469.
[11] C.J. Arnold, T.Q. Ye, R.N. Perutz, R.E. Hester, J.N. Moore, Chem. Phys. Lett. 248 (1996) 464.
[12] M.W. George, T.P. Dougherty, E.J. Heilweil, J. Phys. Chem. 100 (1996) 201.
[13] T.Q. Lian, S.E. Bromberg, M.C. Asplund, H. Yang, C.B. Harris, J. Phys. Chem. 100 (1996) 11994.
[14] S.A. Angel, P.A. Hansen, E.J. Heilweil, J.C. Stephenson, in: C.B. Harris, E.P. Ippen, G. Mourou, A.H. Zewail (Eds.), Ultrafast Phenomena VII, vol. 53 of Springer Series in Chemical Physics, Springer, Berlin, 1990, p. 480.
[15] S.K. Kim, S. Pedersen, A.H. Zewail, Chem. Phys. Lett. 233 (1995) 500.
[16] L. Bañares, T. Baumert, M. Bergt, B. Kiefer, G. Gerber, Chem. Phys. Lett. 267 (1997) 141.
[17] L. Bañares, T. Baumert, M. Bergt, B. Kiefer, G. Gerber, J. Chem. Phys. 108 (1998) 5799.
[18] S.A. Trushin, W. Fuß, W.E. Schmid, K.L. Kompa, J. Phys. Chem. Sect. A 102 (1998) 4129.
[19] S.A. Trushin, W. Fuß, K. Kompa, W.E. Schmid, J. Phys. Chem. Sect. A 104 (2000) 1997.
[20] M. Bergt, N.H. Damrauer, C. Dietl, B. Kiefer, G. Gerber, in: T. Elsaesser, S. Mukamel, M.M. Murnane, N.F. Scherer (Eds.), Ultrafast Phenomena XII, vol. 66 of Springer Series in Chemical Physics, Springer, Berlin, 2001, p. 639.
[21] W.S. Warren, H. Rabitz, M. Dahleh, Science 259 (1993) 1581.
[22] R.J. Gordon, S.A. Rice, Annu. Rev. Phys. Chem. 48 (1997) 601.

[23] S.A. Rice, M. Zhao, Optical Control of Molecular Dynamics, Wiley, New York, 2000.
[24] H. Rabitz, R. de Vivie-Riedle, M. Motzkus, K. Kompa, Science 288 (2000) 824.
[25] M. Shapiro, P. Brumer, in: B. Bederson, H. Walther (Eds.), Advances in Atomic, Molecular, and Optical Physics Advances in Atomic, Molecular, and Optical Physics Series, vol. 42, Academic Press, London, 1999, p. 287.
[26] T. Brixner, N.H. Damrauer, G. Gerber, in: B. Bederson, H. Walther (Eds.), Advances in Atomic, Molecular, and Optical Physics Advances in Atomic, Molecular, and Optical Physics Series, vol. 46, Academic Press, London, 2001, p. 1.
[27] R.S. Judson, H. Rabitz, Phys. Rev. Lett. 68 (1992) 1500.
[28] C.J. Bardeen, V.V. Yakovlev, K.R. Wilson, S.D. Carpenter, P.M. Weber, W.S. Warren, Chem. Phys. Lett. 280 (1997) 151.
[29] A. Assion, T. Baumert, M. Bergt, T. Brixner, B. Kiefer, V. Seyfried, M. Strehle, G. Gerber, in: T. Elsaesser, J.G. Fujimoto, D.A. Wiersma, W. Zinth (Eds.), Ultrafast Phenomena XI, vol. 63 of Springer Series in Chemical Physics, Springer, Berlin, 1998, p. 471.
[30] A. Assion, T. Baumert, M. Bergt, T. Brixner, B. Kiefer, V. Seyfried, M. Strehle, G. Gerber, Science 282 (1998) 919.
[31] T.C. Weinacht, J.L. White, P.H. Bucksbaum, J. Phys. Chem. Sect. A 103 (1999) 10166.
[32] T. Hornung, R. Meier, M. Motzkus, Chem. Phys. Lett. 326 (2000) 445.
[33] M. Bergt, T. Brixner, B. Kiefer, M. Strehle, G. Gerber, J. Phys. Chem. Sect. A 103 (1999) 10381.
[34] T. Brixner, B. Kiefer, G. Gerber, Chem. Phys. 267 (2001) 241.
[35] R.J. Levis, G.M. Menkir, H. Rabitz, Science 292 (2001) 709.
[36] S. Vajda, A. Bartelt, E.-C. Kaposta, T. Leisner, C. Lupulescu, S. Minemoto, P. Rosenda-Francisco, L. Wöste, Chem. Phys. 267 (2001) 231.
[37] C. Daniel, J. Full, L. González, E.-C. Kaposta, M. Krenz, C. Lupulescu, J. Manz, S. Minemoto, M. Oppel, P. Rosenda-Francisco, S. Vajda, L. Wöste, Chem. Phys. 267 (2001) 247.
[38] N.H. Damrauer, C. Dietl, G. Krampert, S.H. Lee, K.H. Jung, G. Gerber, Eur. Phys. J. Sect. D 20 (2002) 71.
[39] T. Brixner, N.H. Damrauer, P. Niklaus, G. Gerber, Nature 414 (2001) 57.
[40] J.L. Herek, W. Wohlleben, R.J. Cogdell, D. Zeidler, M. Motzkus, Nature 417 (2002) 533.
[41] D. Yelin, D. Meshulach, Y. Silberberg, Opt. Lett. 22 (1997) 1793.
[42] T. Baumert, T. Brixner, V. Seyfried, M. Strehle, G. Gerber, Appl. Phys. Sect. B 65 (1997) 779.
[43] A. Efimov, M.D. Moores, N.M. Beach, J.L. Krause, D.H. Reitze, Opt. Lett. 23 (1998) 1915.
[44] T. Brixner, M. Strehle, G. Gerber, Appl. Phys. Sect. B 68 (1999) 281.
[45] D. Zeidler, T. Hornung, D. Proch, M. Motzkus, Appl. Phys. Sect. B 70 (2000) S125.
[46] D. Meshulach, D. Yelin, Y. Silberberg, J. Opt. Soc. Am. Sect. B 15 (1998) 1615.
[47] T. Brixner, A. Oehrlein, M. Strehle, G. Gerber, Appl. Phys. Sect. B 70 (2000) S119.
[48] D. Meshulach, Y. Silberberg, Nature 396 (1998) 239.
[49] T. Hornung, R. Meier, D. Zeidler, K.L. Kompa, D. Proch, M. Motzkus, Appl. Phys. Sect. B 71 (2000) 277.
[50] T.C. Weinacht, J. Ahn, P.H. Bucksbaum, Nature 397 (1999) 233.
[51] R. Bartels, S. Backus, E. Zeek, L. Misoguti, G. Vdovin, I.P. Christov, M.M. Murnane, H.C. Kapteyn, Nature 406 (2000) 164.
[52] J. Kunde, B. Baumann, S. Arlt, F. Morier-Genoud, U. Siegner, U. Keller, Appl. Phys. Lett. 77 (2000) 924.
[53] D.M. Allen, A. Cox, T.J. Kemp, L.H. Ali, J. Chem. Soc. Dalton Trans. (1973) 1899.
[54] L.H. Ali, A. Cox, T.J. Kemp, J. Chem. Soc. Dalton Trans. (1973) 1475.
[55] D.G. Alway, K.W. Barnett, J. Organomet. Chem. 99 (1975) C52.
[56] D.G. Alway, K.W. Barnett, Inorg. Chem. 17 (1978) 2826.
[57] C.E. Borja, V. Jakubek, A.J. Lees, Inorg. Chem. 37 (1998) 5964.
[58] X. Pan, C.E. Philbin, M.P. Castellani, D.R. Tyler, Inorg. Chem. 27 (1988) 671.
[59] R.H. Hooker, K.A. Mahmoud, A.J. Rest, J. Chem. Soc. Dalton Trans. (1990) 1231.
[60] C. Daniel, private communication, 2002.
[61] W.H. Press, S.A. Teukolsky, W.T. Vetterling, B.P. Flannery, Numerical Recipes in C, 2nd ed., Cambridge University Press, Cambridge, 1992.
[62] J.P. Heritage, A.M. Weiner, R.N. Thurston, Opt. Lett. 10 (1985) 609.
[63] A.M. Weiner, D.E. Leaird, J.S. Patel, J.R. Wullert, II, Opt. Lett. 15 (1990) 326.
[64] A.M. Weiner, D.E. Leaird, A. Patel, J.R. Wullert, II, IEEE J. Quantum Electron. 28 (1992) 908.
[65] M.M. Wefers, K.A. Nelson, Opt. Lett. 20 (1995) 1047.
[66] M.M. Wefers, K.A. Nelson, J. Opt. Soc. Am. Sect. B 12 (1995) 1343.
[67] A.M. Weiner, Rev. Sci. Instrum. 71 (2000) 1929.
[68] D.E. Goldberg, Genetic Algorithms in Search, Optimization, and Machine Learning, Addison-Wesley, Reading, 1993.
[69] H.-P. Schwefel, Evolution and Optimum Seeking, Wiley, New York, 1995.
[70] J.E. Huheey, E.A. Keiter, R.L. Keiter, Anorganische Chemie, Walter de Gruyter, Berlin, 1995.